

Top-Down Approach to Study Chemical and Electronic Properties of Perovskite Solar Cells: Sputtered Depth Profiling Versus Tapered Cross-Sectional Photoelectron Spectroscopies

Chittaranjan Das,* Waqas Zia, Claudiu Mortan, Navid Hussain, Michael Saliba,* Jan Ingo Flege, and Małgorzata Kot*

A study of the chemical and electronic properties of various layers across perovskite solar cell (PSC) stacks is challenging. Depth-profiling photoemission spectroscopy can be used to study the surface, interface, and bulk properties of different layers in PSCs, which influence the overall performance of these devices. Herein, sputter depth profiling (SDP) and tapered cross-sectional (TCS) photoelectron spectroscopies (PESs) are used to study highly efficient mixed halide PSCs. It is found that the most used SDP-PES technique degrades the organic and deforms the inorganic materials during sputtering of the PSCs while the TCS-PES method is less destructive and can determine the chemical and electronic properties of all layers precisely. The SDP-PES dissociates the chemical bonding in the spiro-MeOTAD and perovskite layer and reduces the TiO_2 , which causes the chemical analysis to be unreliable. The TCS-PES revealed a band bending only at the spiro-MeOTAD/perovskite interface of about 0.7 eV. Both the TCS and SDP-PES show that the perovskite layer is inhomogeneous and has a higher amount of bromine at the perovskite/ TiO_2 interface.

short investigation time. The outstanding outcome of PSCs encourages the community to upscale and commercialize this technology. Rapid developments in PSCs came from the possibilities to tune the absorber layer's optoelectronic properties by changing the chemistry and the selective contact layers in these devices. For high performance, tandem solar cell technology and long-term stability, an experimental study on the correlation of layers and interface chemistry is necessary. However, long-term stability related to bulk and interface chemistry is still an issue for this technology, which is often overlooked.

Various methods have been used to improve the PSCs' efficiency and stability. The chemistry of interfaces has been often modified to improve their performance and stability.^[1–4] For example, the authors have already tried to understand the correlation

between interface design and the performance of solar cells.^[2] They found that the interface chemistry and band alignment depend on the interface design.^[2] The electronic and chemical properties of the film in the bulk and at interfaces in the

1. Introduction


Organic–inorganic hybrid perovskite solar cells (PSCs) achieved a remarkable performance of 25.5% efficiency in very

C. Das
Karlsruher Institut für Technologie (KIT)
Institute for Applied Materials-Energy Storage Systems (IAM-ESS)
76344 Eggenstein-Leopoldshafen, Germany
E-mail: chittaiit@yahoo.com

W. Zia, C. Mortan, M. Saliba
Institut für Photovoltaik
Universität Stuttgart
70569 Stuttgart, Germany
E-mail: michael.saliba@ipv.uni-stuttgart.de

N. Hussain
Karlsruher Institut für Technologie (KIT)
Institute of Nanotechnology
P.O. Box 3640, 76021 Karlsruhe, Germany

J. Ingo Flege, M. Kot
Chair of Applied Physics and Semiconductor Spectroscopy
BTU Cottbus-Senftenberg
03046 Cottbus, Germany
E-mail: sowinska@b-tu.de

 The ORCID identification number(s) for the author(s) of this article can be found under <https://doi.org/10.1002/solr.202100298>.

© 2021 The Authors. Solar RRL published by Wiley-VCH GmbH. This is an open access article under the terms of the Creative Commons Attribution-NonCommercial-NoDerivs License, which permits use and distribution in any medium, provided the original work is properly cited, the use is non-commercial and no modifications or adaptations are made.

DOI: 10.1002/solr.202100298

PSCs are often studied directly using various microscopic and spectroscopic methods.^[5,6] In particular, time of flight secondary ion mass spectroscopy (ToF-SIMS), transmission electron microscopy (TEM)^[7–10] and field emission secondary electron microscopy (FESEM)^[11] are used. The distribution of organic and inorganic cations has been determined over the whole thickness of the mixed cation-based PSCs using ToF-SIMS. Ducati et al. carried out TEM measurements on PSCs to determine the films' quality concerning chemical homogeneity, morphology, and efficiency.^[12–14] Both, TEM and ToF-SIMS methods, effectively study bulk and interfaces' chemistry but without giving any information about the electronic properties of the PSCs stack. The microscopic techniques such like Kelvin probe force microscopy (KPFM) and scanning tunneling microscopy (STM) are useful for addressing the device's charge dynamics at interfaces.^[8,15–17] However, KPFM and STM are not sensitive to the chemistry of the layers.

A method of choice that can determine the chemistry of the layers with their electronic properties at interfaces is PES.^[18] PES studies have been mostly done on the single crystal surfaces or at the interface using the sequential deposition of over-layer film.^[5,6,19,20] There are also few studies where a special type of PES, namely, hard X-ray photoelectron spectroscopy (HAXPES), and sputter depth profiling PES (SDP-PES), were used to study bulk of the PSCs. HAXPES uses synchrotron radiation, i.e., a tunable X-ray source, where the photon energy can be adapted to selectively increase or decrease the surface sensitivity of the measurements. In HAXPES studies, Philippe et al. have found in state-of-the-art Rb-doped triple cation (Cs, formamidinium [FA], methylammonium [MA]) that perovskites have higher Cs concentration is deep in the film while the surface is rich in formamidinium iodide (FAI).^[21] The TiO₂/perovskite interface studied by HAXPES revealed that the conduction band minima (CBM) and valence band maxima (VBM) of the TiO₂ film are located 0.4 and 2.1 eV below the perovskite CBM and VBM, respectively.^[22] Despite these findings at the surface and in the perovskite bulk HAXPES is limited to a thickness of around 50 nm at maximum only, which is still far from the thickness of PSCs devices. Another disadvantage of the HAXPES method is that currently these measurements can essentially only be carried out at synchrotrons, resulting in very limited availability.

Next, to study chemical and electronic properties from top to the bottom contact of the PSCs SDP-PES has been used.^[23–26] Noël et al. have shown that the chemical distribution of perovskites can be studied with SDP-PES; however, the sputtering process degrades the material itself, inducing the formation of metallic lead,^[23,24] causing ambiguities in the analysis. In another work, Eom et al., have studied the interfaces of PSCs.^[25] The modification of the electron transporting layer due to sputtering, especially of the TiO₂, made the analysis unreliable. To overcome the substrate degradation caused by sputtering, recently the mechanical process of etching has been tried by various groups to study the chemistry of the entire PSCs.^[27–29]

In this work, we used two different top-down processing approaches to analyze the chemical and electronic properties of the PSC stack. Low Ar⁺ sputtering energy SDP-PES is compared with the mechanically prepared tapered cross-sectional PES (TCS-PES). It is found that the low energy SDP-PES method

alters the chemistry of the perovskite and TiO₂ layers and their electronic properties. The TCS-PES method does not change the chemistry of the films and thus the band alignment can be investigated properly, but carbon, nitrogen, and oxygen, as contaminations adsorbed on each layer surface, are present across all films in the PES spectra and for the chemical analysis these spectra need to be fitted carefully and exclude the effect of contamination. The TCS-PES partially destroys the device and retains the chemical and electronic properties of the PSC stack while the SDP-PES is able to define the point of layer transition in the PSC stack and the elemental concentration in each layer. Therefore, we recommend the use of both methods to fully understand the chemical and electronic properties of the investigated PSCs.

2. Results and Discussion

2.1. Spectral Analysis

A classical n–i–p-type structure of the PSC was used in this study. Going from the PSC bottom to the top one can distinguish: n-type TiO₂ (200 nm), perovskite (450 nm), spiro-MeOTAD (150 nm), and Ag (100 nm) used as electron-transport layer (ETL), absorber, hole-transporting layer (HTL), and metal contact, respectively. Each of this top-down approach to measure various layers of PSC takes 5–6 h. Such a prolonged X-ray expose may cause a change in chemical properties of the perovskite layer itself. However, in our previous studies, we found that the perovskite is stable under X-ray exposer under the vacuum unless any external factor such as heat, moisture, or visible light is provided to the system.^[19,23,30–34]

The same PSC composition was once investigated using SDP-PES (Figure 1a) and once using TCS-PES (Figure 1b). In Figure 1, on all abscissae, the binding energy of the selected chemical element's core level is shown. On the abscissae in the SPD-PES results, the etching time (Figure 1a), and in the TCS-PES the depth (Figure 1b) are shown. The color scale going from black to white marks the intensity of the respective element, while black stands for the zero/or minimum and white for the maximum intensity.

In the SDP-PES study (Figure 1a), a PSC stack was sputtered with Ar⁺ ions having an energy of 500 eV, and subsequently the SDP-PES spectra were collected. Each sputter step lasted for 200 s. The red lines through the contour plots mark the main peak binding energy of each core level. As can be seen, after the metallic contact has been sputtered, the peaks shift initially toward higher and then toward lower binding energy. In general, the binding energy shift may originate from different sources such like X-ray illumination (charging) and/or the electronic properties of the layers. We will discuss this in detail hereafter.

The binding energy of the Ag3d_{5/2} is located at 368.2 eV confirming that the Ag contact is metallic.^[35] The binding energy position of the Ag3d_{5/2} can be considered as the reference level for further analysis of other spectra. The intensity of the Ag3d_{5/2} decreases after about 20 min of sputtering and almost vanishes after around 40 min being slightly detected until about 55 min. The binding energy of the C1s is located at 285.4 eV and can be attributed to the organic carbon.^[36] After the first sputtering step,

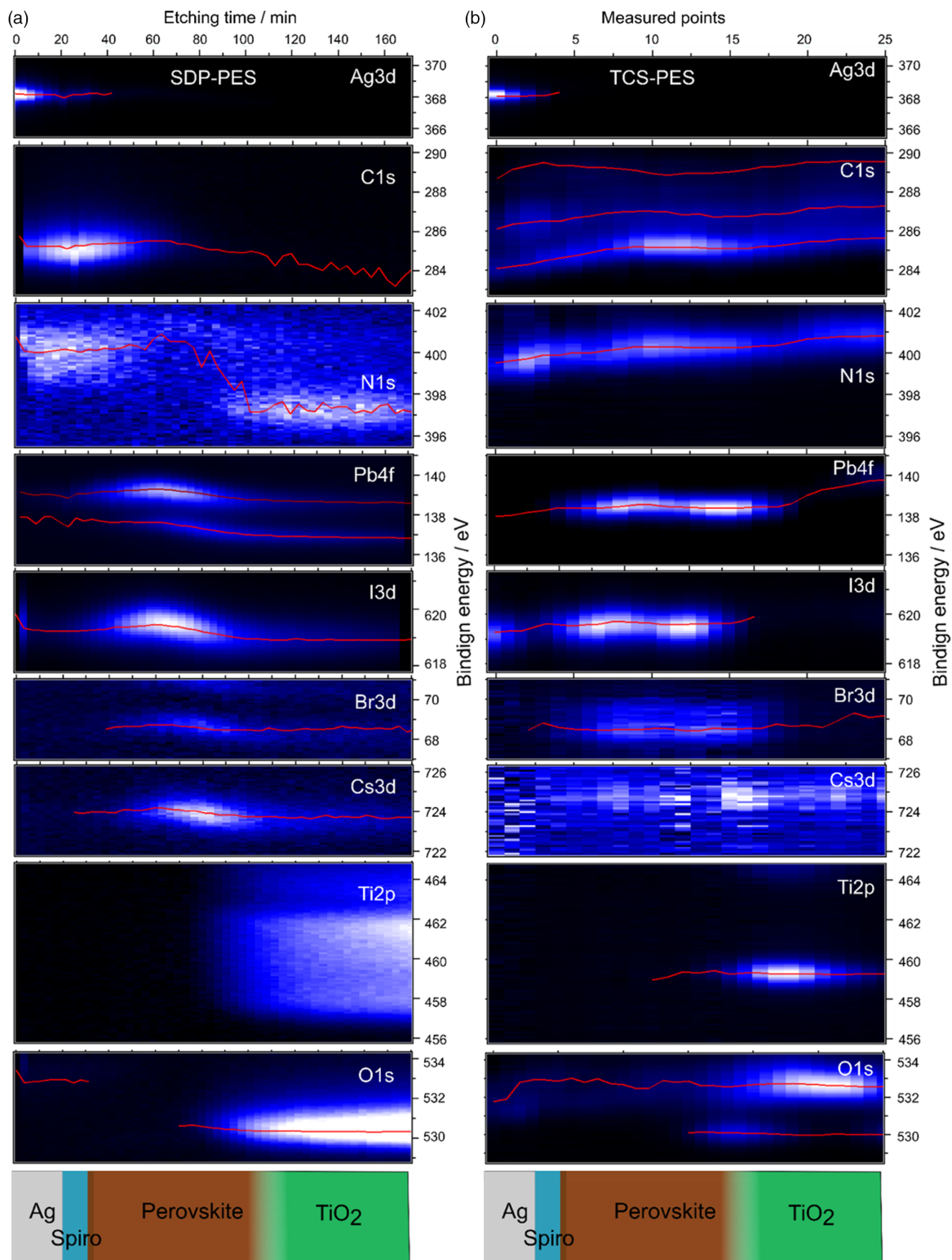


Figure 1. Contour plot representation of the $\text{Ag}3d_{5/2}$, $\text{C}1s$, $\text{N}1s$, $\text{Pb}4f_{7/2}$, $\text{I}3d_{5/2}$, $\text{Br}3d_{5/2}$, $\text{Cs}3d_{5/2}$, $\text{Ti}2p_{3/2}$, and $\text{O}1s$ core-level spectra investigated using a) SDP-PES (left) and b) TCS-PES (right) methods and plotted along the depth of the PSC stack. The vertical axes show the electron binding energy of the individual spectra; a) the horizontal axes either denote the etching time or b) the measured points on the tapered cross section. The color scale shows the core-level intensity going from minimum or zero (black) to the maximum (white). The red lines in all contour plots highlight the peak positions of respective core level determined from the fitting of individual spectra.

the C1s intensity starts to increase and decreases after 60 min. The N1s has a steady intensity till 60 min of sputtering and after that it decreases until 100 min reaching again steady intensity until the end of sputtering. The N1s has a binding energy located at 400.0 eV at the surface and it continues till sputtering of 60 min which resembles the nitrogen contribution from the spiro-MeOTAD (see Figure S1, Supporting Information).^[37] After 100 min of sputtering, another intense peak appears at the binding energy of 397.0 eV. This peak at 397.0 eV could be related to a new species or sputtering related damage, which will be discussed hereafter. The Pb4f_{7/2} and I3d_{5/2} spectra have already very low intensities on the Ag side that start to increase after etching for 20 min. The Pb4f_{7/2} has two clearly visible peaks located at 138.9 and 137.7 eV that correspond to the Pb²⁺ and Pb⁰ states.^[38,39] The I3d_{5/2} spectra have a binding energy at around 619.5 eV corresponding to the iodine in perovskite (see Figure S1, Supporting Information).^[40,41] The intensity of the Cs3d_{5/2} and Br3d_{5/2} core levels starts to increase after 50 min of sputtering and decreases after 100 min. The binding energy of the Cs3d_{5/2} and Br3d_{5/2} (723.9 and 68.6 eV) is attributed to the binding energy of the investigated perovskite film shown in Figure S1, Supporting Information.^[40] The Ti2p_{3/2} and O1s intensities start increasing at around 90 min of sputtering and get highest intensity after 100 min of sputtering. The Ti2p_{3/2} spectrum is very broad, making it difficult to assign any binding energy position and rendering peak deconvolution necessary. Such a broad Ti2p peak presumably indicates changes in the oxidation state of titanium by sputtering as this effect was also observed in other Ar⁺-sputtered TiO₂ films in the literature.^[24,25] The most intense O1s peak exhibits a binding energy of 530.3 eV after 100 min of sputtering that corresponds to the Ti–O bond,^[42–44] but it gets also broader with the sputtering time. In addition to that, a peak having lower intensity but higher binding energy (532.6 eV) is visible at the early stage of sputtering and can be attributed to the adsorbed –OH groups on the surface.

The interfaces between the different layers of the PSC's stack can be identified analyzing the spectral intensity of all core levels in the collected SDP-PES data. Namely, a decrease in the peak intensity related to an overlayer is accompanied by an increase in the peak intensity related to the layer underneath and their interface. In our SDP-PES studies, the first interface reached is between Ag and the spiro-MeOTAD layers. The Ag3d_{5/2} peak intensity decreases and the C1s and N1s intensities increase after about 20 min of sputtering. The C1s and N1s spectra do not change their intensity until about 50 min of sputtering, as expected by the presence of the spiro-MeOTAD layer. The parallel increase in intensities of Pb4f_{7/2} and I3d_{5/2} after about 50 min marks the interface to the perovskite layer underneath. The strong intensity of the Br3d_{5/2} and Cs3d_{5/2} peaks starts a bit later (after 60 min) and can be related to the lower sensitivity of the PES to these core levels or different concentration of those elements at the interfaces. Interestingly, a high I3d_{5/2} intensity is also observed at the Ag layer as well as lower intensity across it and spiro-MeOTAD film. Indeed, iodine is known to migrate into the PSC stacks.^[45–47] The perovskite/TiO₂ interface seems to be rather broad. The signal related to the perovskite core levels seems to sharply decrease after 90–100 min, but the strong Ti2p or O1s arises 10–15 min later. This shows that after 90 min of sputtering the mesoporous perovskite-TiO₂ interface is reached

and on further sputtering (after 110–115 min) a compact TiO₂ layer is found. The SDP-PES shows that the interface of Ag/spiro, spiro/perovskite, and perovskite/TiO₂ is reached after 20, 50, and 90 min of sputtering, respectively. However, unlike conventional approach of interface measurement by X-ray photoelectron Spectroscopy (XPS) here the exact interface determination is not possible due to the preferential etching of various layers. The SDP-PES shows that the interface of Ag/spiro, spiro/perovskite, and perovskite/TiO₂ is reached after 20, 50, and 90 min of sputtering, respectively. However, unlike conventional approach of interface measurement by XPS here the exact interface determination is not possible due to the preferential etching of various layers. The SDP-PES shows that the interface of Ag/spiro, spiro/perovskite, and perovskite/TiO₂ is reached after 20, 50, and 90 min of sputtering, respectively. However, unlike conventional approach of interface measurement by XPS here the exact interface determination is not possible due to the preferential etching of various layers.

In Figure 1b, the core-level spectra of the Ag3d_{5/2}, C1s, N1s, I3d_{5/2}, Pb4f_{7/2}, Br3d_{5/2}, Cs3d_{5/2}, Ti2p_{3/2}, and O1s collected on the tapered cross-section of a complete solar cell stack are shown. The TCS-PES measurement was carried out along the solar cell stack going from the Ag top to the TiO₂ bottom contact. The Ag3d_{5/2} peak measured with TCS-PES is also located at the binding energy of 368.2 eV that corresponds to the metallic Ag.^[36] As expected, the Ag intensity is higher on the surface (point 1) and starts to decrease after measurement point 3. Ag3d_{5/2} peak vanishes completely around measurement point 5. The C1s peak is already visible in the surface-sensitive measurement, which is typical for a sample that was briefly exposed to air and stored in a glovebox before the PES measurement. The C1s spectral intensity starts to rise after the measurement point 3, where the Ag3d_{5/2} starts to decrease. The C1s spectrum has three main peaks located at 284.0, 286.0, and 288.6 eV. These binding energies may correspond to spiro-MeOTAD, perovskite, and/or to an adsorbed carbon on the sample.^[27,36,48] The N1s, I3d_{5/2}, and Pb4f_{7/2} have main peak binding energies located at around 399.1, 619.5, and 138.4 eV (also see Figure S2, Supporting Information, for a pristine perovskite film). Similar binding energies on the TCS-PES have been observed in previous reports.^[27,29] The N1s intensity starts to increase just after the first measurement point and maintains a constant intensity parallel to the intensity profile of C1s until point 25, which can be related to the adsorption of C and N on the TCS-PSC surface and/or from the perovskite layer. I3d_{5/2} and Pb4f_{7/2}, which are elements of the investigated perovskite film, start to increase at point 5, which continues until point 17. Within the point interval from 0 to 5, the Pb4f_{7/2} has a negligible intensity where the I3d_{5/2} has certain intensity which might have come from the iodide migration to the metal contact.^[49] The parallel change in the intensity of I and Pb elements shows that the point 5 is the starting point of the perovskite layer on the tapered cross section. Unlike the SDP-PES, the Pb⁰ state is absent on the TCS-PES suggesting that the sputtering causes the reduction to metallic lead. The Br3d_{5/2} peak located at the binding energy of 68.5 eV from measurement point 5 until point 20 shows the presence of Br from the solar cell. Looking at the data shown in Figure 1b, it is observed that the Br intensity rises abruptly just after the Ag intensity. The Cs3d_{5/2} has a binding energy of 724.7 eV

and a very low signal-to-noise ratio. This may come from the low concentration (0.05) of Cs in the investigated perovskite. Even if the concentration is low, the TCS-PES is able to detect the presence of Cs in the perovskite film. The intensity increase in $Cs3d_{5/2}$ starts around point 5 and continues until point 17. The O1s and Ti2p core level spectral intensities start to increase at point 15 and continue to increase until point 25. The Ti2p_{3/2} core level is very sharp and is located at 459.8 eV corresponding to the binding energy of TiO₂.^[50,51] The O1s has two peaks located at 530.0 and 532.6 eV. The higher binding energy (532.6 eV) peak is found all over the TCS profile, whereas the lower binding energy peak appears at around point 15 along with the Ti2p. Interestingly, the higher binding energy O1s peak has binding energy at around 532.2 eV at Ag interface, which can come from the spiro-MeOTAD layer^[48] whereas the higher binding energy O1s at the TiO₂ end can be attributed to the -OH groups absorbed on the surface.^[52] In the TCS-PES (Figure 1b), the contour plot shows that the Ag/spiro-MeOTAD interface is located at around measurement point 3, the spiro-MeOTAD/perovskite at around point 5 and the perovskite/TiO₂ at around the measurement point 15.

2.2. Elemental Distribution across the PSCs

The distribution of all elements across the PSC stack can be determined from the analysis of both the SPD- and TCS-PES data. The elemental analysis identifies different interfaces and shows how the chemistry of individual layers changes across the PSC stack. In Figure 2, the atomic concentration of various elements present in the investigated PSC stack is determined from the SDP- (Figure 2a) and TCS-PES (Figure 2b) data shown in Figure 1.

The elemental distribution of the chemical elements determined from the SDP-PES results (Figure 2a) shows that the metal contact surface, in addition to silver is also rich in carbon (22 at%) and iodine (10 at%). Also here, it is worth to mention that the XPS method is very surface sensitive and can inform

about 6–10 nm of depth from surface. However, what is absorbed on the surface will strongly contribute to the spectra without any sputtering. In a case of sputtering, the surface layer is removed and the layer underneath is measured. The elemental concentration of various layers in the SDP-PES is shown in Figure 2a. The XPS method is also able to determine the PSC cross-sectional elemental composition when a taper cut from Au to TiO₂ layer is made. However, the cross-contamination during the sample preparation causes certain uncertainties in the quantification of the relative C and N concentrations in the PSC stack. A list detailing the concentration of each element in certain depths is shown in Table 1. Generally, the presence of carbon on any substrate surface is not surprising as one can always find carbon in the PES spectra, when samples are taken from ambient environment to vacuum.^[48] But, the presence of iodine suggests that the iodine ions have migrated through the spiro-MeOTAD film toward the surface. After 20 min of sputtering the Ag concentration sharply decreases, whereas the carbon concentration increases to 60% showing the interface of Ag/spiro-MeOTAD. Nitrogen, one of the main components in the spiro-MeOTAD, should have a similar concentration like carbon. However, after 20 min of sputtering nitrogen exhibits a very low concentration, and also the nitrogen concentration remains very low until the end of the sputtering step through the perovskite. After 40 min of etching, carbon decreases sharply while the concentrations of the other elements from the perovskite (Pb, I, Br, and Cs) increase and then, after 63 min of etching, start to decrease again. The titanium and oxygen contributions start to increase after 73 min of etching showing the presence of perovskite in the mesoporous TiO₂. In addition, the carbon concentration gradually decreases across the perovskite film (40–90 min). Around 63 min, the I, Pb, Br, Cs, and N concentrations amount to 35.5, 30.3, 13.1, 4.4, and 0.4 at%, respectively. The ideal relative concentrations of I, Pb, Br, Cs, and N in the mixed perovskite [Cs_{0.05}(FA_{0.83}MA_{0.17})_{0.95}Pb(I_{0.83}Br_{0.17})₃] are 33.2, 13.3, 6.8, 0.7, and 23.0 at%, respectively. The XPS measurement on the surface of the perovskite film shows a relative ratio of 7.2, 21.3, 4.5, 21.1,

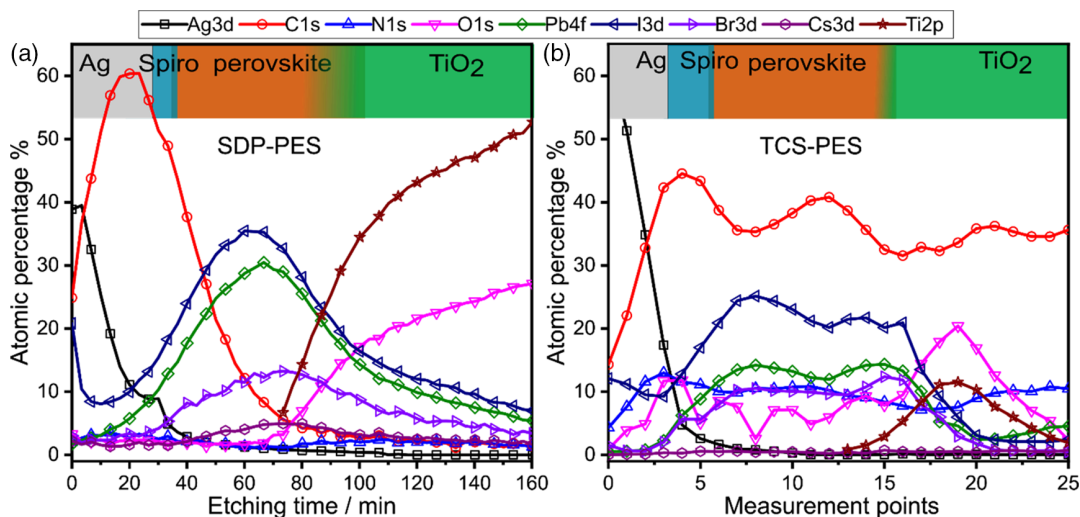


Figure 2. The elemental concentration across the PSC from Ag to TiO₂ layer determined from the a) SDP-PES and b) the TCS-PES data shown in Figure 1. A schematic structure of a solar cell presented on the top of each figure shows the equivalent positions of elements in the complete solar cell.

Table 1. The atomic concentration of PSC over from Ag to TiO₂ contacts obtained by SDP-PES and TCS-PES.

Elements	Ideal at% in perovskite	Atomic percentage (%) of elements							
		Etching time (min) in SDP-PES				Measured points on TCS-PES			
		0–30	30–55	55–100	100–160	0–4	4–15	15–20	20–25
Ag		40–9	9–0			62–5	5–0		
Pb	13.3	0–8	8–27	27–14	14–5	0–5	5–14	14–3	3–4
I	33.2	17–15	15–27	27–16	16–7	10–11	11–21	21–4	4–3
Br	6.8	0–4	4–11	11–9	9–3	0–5	5–12	12–2	0
N	23.0	0–3	3–1	1–2	2–1	5–11	11–8	8	8
C	23.0	24–53	53–17	17–3	3–2	14–43	43–31	31–35	35
Cs	0.7	0	4	3	1.2	0–0.8	0.8	–	0.9
Ti				0–34	34–52	–	–	2.8–10	10–3
O		2	2	2–17	17–27	0–10	10–8	10–17	17–3

37.1, 0.5, and 8.3 for Pb, I, Br, N, C, Cs, and O. The elemental concentration differs from the ideal values due to the fact that the samples are exposed to air and can absorb oxygen and carbon from the atmosphere. The SDP-PES shows that the Pb, Br, and Cs concentrations are higher than the expected values, whereas I, C, and N are far below the ideal concentration. The unexpected concentration of chemical elements in the perovskite film indicates that the sputtering process might have caused damage to the chemistry of the layers. Toward the front of TiO₂ contact, the atomic concentration of Ti and O shows a wrong ratio of about 2:1 between them. The elemental concentration in the SDP-PES of PSC shows that the organic components and iodine are removed from the solar cell quickly during sputtering.

The atomic concentration across the PSC stack (shown in Figure 2b) from TCS-PES shows the presence of carbon and iodine on the silver surface amounting to 15% and 12% as well as across the Ag and the spiro-MeOTAD layers. The carbon concentration increases just after the first measuring point and stays almost unchanged throughout the measurement. Moreover, nitrogen exhibits the same trend as carbon. Deviating from the nominal solar cell stack composition, this unexpected consistency in carbon and nitrogen concentrations across the whole PSC stack originates from the cross-contamination during the TCS preparation. After measurement point 5, the relative concentrations of the perovskite elements (Pb, I, Br, and Cs) increased to 14.0, 21.0, 12.0, and 0.8 at%, respectively, and remained unchanged until point 15. The Pb, I, and Cs concentrations are closer to the ideal concentration of the perovskite studied here, whereas Br has higher contents. In our previous studies also, it was found that the mixed halide perovskite has a higher Br concentration in the perovskite.^[27,29] The stoichiometric presence of perovskite elements at point 5 and onward, shows this point can be interpreted as the transition point from Ag to perovskite through the spiro-MeOTAD. The Ti and O atomic concentrations start to increase after point 15 until point 20. At point 20, the Pb, I, and Br concentrations vanish, thereby marking the starting point of the compact TiO₂. Therefore, point 15 remarks the start of the perovskite/mesoporous TiO₂ interface with substantial intermixing; from point 20 onward the compact TiO₂ layer of the PSC stack has been reached. Concluding this

section, the atomic concentrations of the various elements on TCS could easily be quantified including the identification of the respective interfaces. Also, the process does not modify or even destroy the perovskite or any other layer of the PSC stack. Here, we would like to mention that the XPS method being surface sensitive is able to determine the PSC cross-sectional elemental composition when taper cut from Au to TiO₂ layer. However, the cross-contamination during the sample preparation causes certain uncertainties in the quantification of the relative C and N concentrations in the PSC stack.

2.3. Elemental Composition of the Perovskite and TiO₂ Layers

The atomic ratio of different elements in the device can help us to understand the material chemistry in the layer. In the previous section in Figure 2, we discuss about the elemental concentration determined from the SDP- and TCS-PES measurements. Here, we want to focus on the chemical properties of the perovskite and TiO₂ layers in the device.

In the TiO₂, the Ti:O ratio in the SDP-PES results is found to be around 2, which is far away from the ideal ratio of 1:2 (shown in Figure 3a). In the perovskite precursor, the Br:I ratio is 0.2:1 (so 0.2). In an ideal case, this ratio shall be maintained in the perovskite film. However, the Br:I ratio (Figure 3b) in the SDP-PES method shows a gradual increase from 0.27 to 0.5 toward perovskite/TiO₂ interface. This means that the back contact (spiro-MeOTAD/perovskite interface) has a higher concentration of iodine, whereas the front contact (perovskite/TiO₂ interface) has a higher bromine concentration. In our previous studies, we have observed similar trends in the mixed perovskite-based solar cells.^[27,29] In the SDP-PES results, the atomic ratio of lead to halide (Figure 3c) is found to be about 6–2 from top (Ag) to bottom (TiO₂) contact. From Figure 3c, it is evident that the halide concentration is lower than the expected value for the investigated perovskite film. This lower concentration of iodine could come from the sputtering-induced degradation of the perovskite film in the PSC stack.

In the TCS-PES method, the lead to halide ratio (Figure 3f) is found to be about 1:3.2 to 1:2.9, which is close to the ideal ratio of 1:3. The Pb:(I + Br) does not change much from point 5 till point

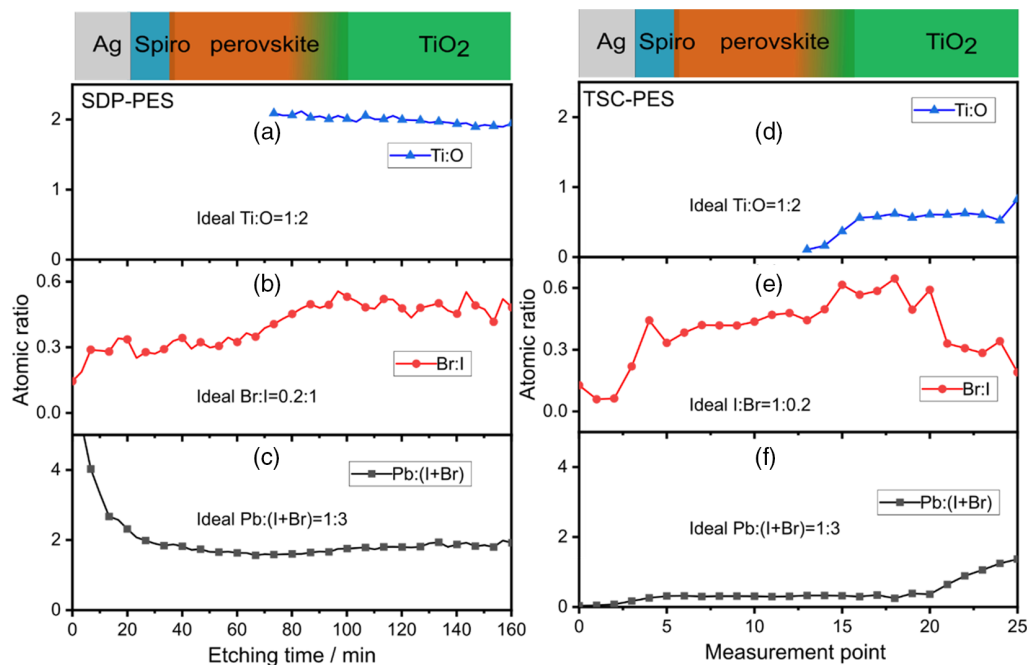


Figure 3. The atomic ratio of a,d) Ti:O, b,e) I:Br, and c,f) Pb to halide [Pb:(I + Br)], in the a–c) SDP and d–f) TCS-PES.

17 showing the exact place of the perovskite layer on the TCS. In Figure 3e, the Br:I ratio on the TCS is found to increase gradually from back (0.3) to front (0.6) contact. A similar finding was reported in our previous work using TCS-PES^[27,29] to investigate mixed perovskite film, which showcases the reproducibility of this technique in different laboratories and of the samples prepared by different groups. At the front contact, the Ti:O ratio (Figure 3d) on the TCS is found to be around 0.6, which is close to the ideal value of 0.5 for stoichiometric TiO₂.

When comparing the respective atomic ratios of the individual elements extracted from the SDP- and TCS-PES results, the perovskite film has a lower concentration of halide as derived from SDP-PES. This lower concentration may have evolved from the sputtering-related degradation causing the perovskite to form lead halide.^[53] The Ti:O ratio in the SDP-PES shows that the sputtering artificially increases the Ti concentration in the TiO₂ layer, whereas in the TCS-PES, it is unchanged.

Irrespective of the used investigation method, the bromine concentration is found to be higher at the perovskite/TiO₂ interface, whereas the iodine concentration is higher at the spiro-MeOTAD/perovskite interface.

2.4. Chemical Properties of the Perovskite and TiO₂ Layers

The electronic properties at the interfaces^[49,50] are the factors responsible for the performance of the photovoltaic devices.^[51,52] These factors are intimately related to the changes in the chemistry of the layers at the interfaces, which can be determined with PES.^[53–55] In Figure 4a,c, C1s and Pb4f_{7/2} core-level spectra are presented that were collected at the Ag surface, the spiro-MeOTAD/perovskite interface, and in the middle of the

perovskite layer using SDP-PES. The C1s peak shape on the Ag surface (Figure 4a, top) has an intense peak at around 285.0 eV corresponding to C–C bond and two other peaks at 286.8 and 288.7 eV corresponding to the absorbed carbon, C=O and –O–C=O species, respectively.^[56] The C1s spectra at the spiro-MeOTAD/perovskite and in the middle of the perovskite film surface look very similar to the one collected on the Ag surface. Moreover, the detected features do not match with that of spiro-MeOTAD and/or perovskite. In addition, the carbon intensity decreases in the perovskite film, contrary to the expectation, as the perovskite should have a significant carbon contribution in the film bulk.

Next, the C1s core level investigated with TCS-PES is fitted with six peaks labeled as A–F in Figure 4b. The C1s spectra have resemblance with the pure spiro C1s spectra shown Figure S1, Supporting Information. The peaks are originated from the carbon atom bonded to hydrogen, carbon, oxygen, and nitrogen in the spiro-MeOTAD molecule (see Figure S1, Supporting Information). The fitted peaks in C1s originated from C–H (A), spiro C–C (B), C–N (C), aromatic C–O (D), C–O (E),^[27] and C–F (F). Here the C1s spectra related to spiro moved to lower binding energy due to the doping of spiro-MeOTAD with LiTFSI.

However, one should not find any spiro-MeOTAD on the thick Ag layer. The mechanical surface preparation might be responsible for that. Moving further along the tapered cross-section the main peak shifts to higher binding energy 284.5 eV, which is caused by the interface band bending from the spiro-MeOTAD to the perovskite layer.^[27,29] Moving along the TCS at the perovskite layer, the C1s has three peaks 285.0, 286.8, and 288.7 eV, which correspond to the C1s spectra of the investigated perovskite.^[57] Comparing the C1s from SDP and

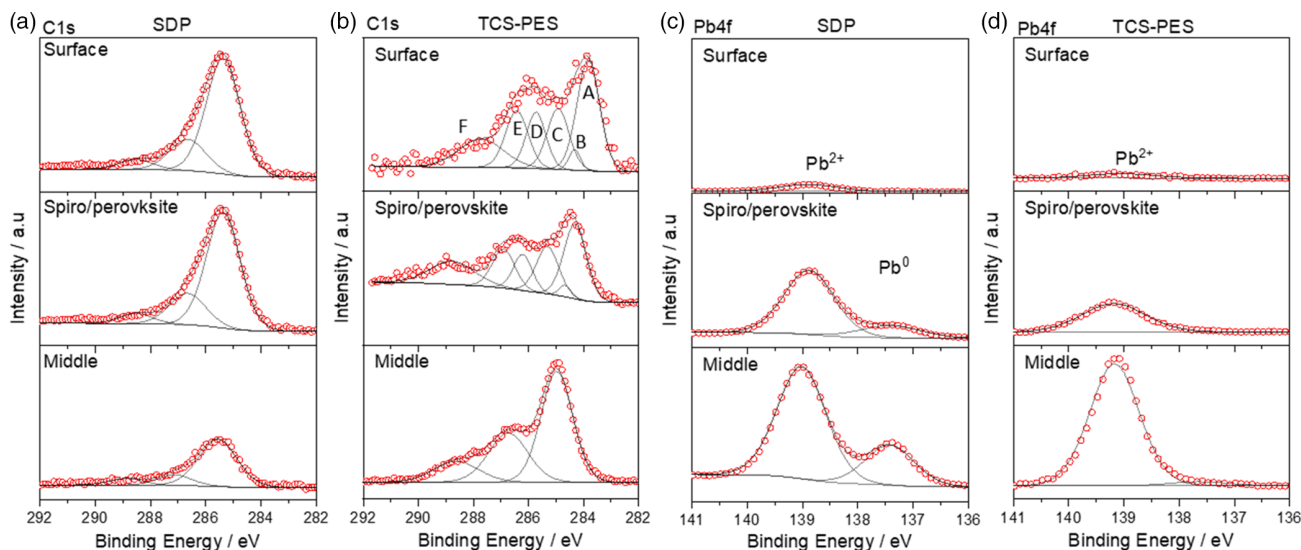


Figure 4. Evolution of the a,b) C1s and c,d) Pb4f_{7/2} core-level spectra at the surface (top), spiro-MeOTAD/perovskite interface (middle), and in the middle of the perovskite film (bottom) investigated using a,c) SDP- and b,d) TCS-PES methods.

TCS-PES one can conclude that the organic part of the solar cell degrades under the influence of sputtering. The C1s spectra investigated using SDP-PES have much broader peaks than using TCS-PES indicating again a destructive influence of the sputtering on the investigated layers.

In Figure 4c,d, the Pb4f spectra from SDP- and TCS-PES taken on the surface, interface, and perovskite layer are compared. It can be seen that in both cases, a small intensity of lead is detected on the Ag surface. At the interface of spiro-MeOTAD/perovskite, the intensity of Pb4f_{7/2} starts to increase in both cases. In case of SDP-PES, a peak at lower binding energy (137.4 eV) appears that corresponds to metallic lead, whereas in case of TCS-PES, this peak is not visible. In the SDP-PES, the intensity of the metallic Pb4f_{7/2} peak (137.4 eV) increases with sputtering, which clearly illustrates the degradation of the perovskite.^[38] That metallic lead

is missing in TCS-PES at the perovskite layer indicates yet again that sputtering is a destructive method and may lead to a wrong interpretation of the data.

The a,c) Ti2p and b,d) O1s spectra collected using a,b) SDP-PES and c,d) TCS-PES methods at the perovskite/TiO₂ interface (top) and in the middle of the TiO₂ film (bottom) are shown in **Figure 5**. In Figure 5a, in both investigated places, the Ti2p core level shows very broad spectrum. The Ti2p spectrum has to be deconvoluted using four doublets that can be assigned to Ti⁴⁺, Ti³⁺, Ti²⁺, and Ti⁰⁺ states.^[58–61] The peaks located from 452.0 to 461.0 eV come from the Ti2p_{3/2} spin orbit and the peaks of the second spin orbit of Ti2p_{1/2} are located from 461.0 to 467.0 eV (shown in Figure 5a). The appearance of multiple chemically shifted components in the Ti2p core level clearly shows that the TiO₂ underneath the perovskite is reduced to titanium

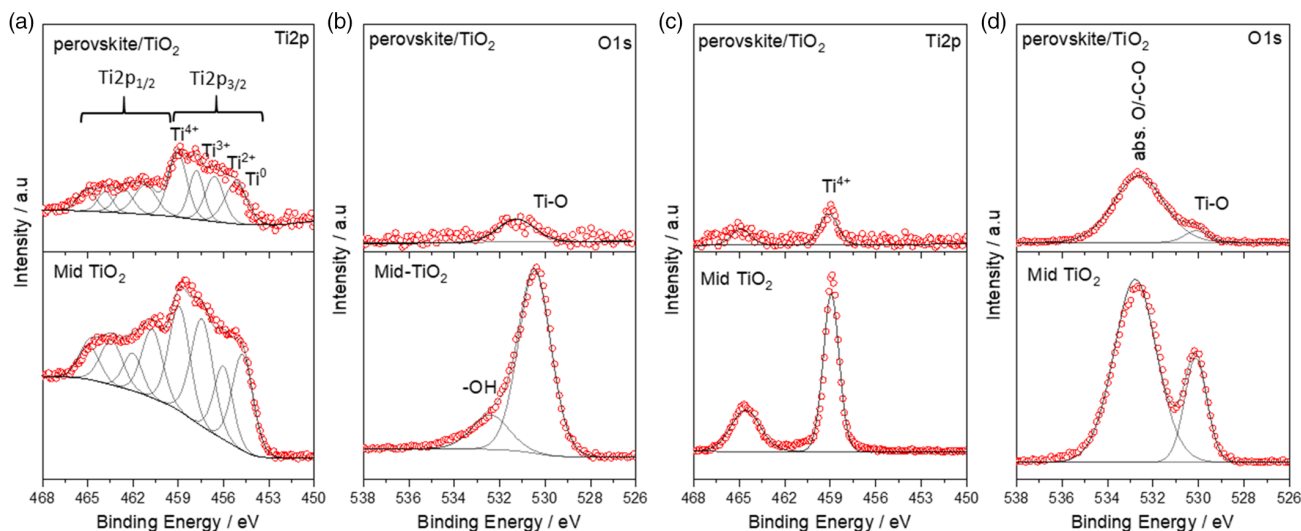


Figure 5. Ti2p and O1s from the perovskite/TiO₂ interface (Interface/TiO₂), and from TiO₂ layer (Mid-TiO₂) from a,b) SDP-PES and c,d) TCS-PES.

suboxides. The reduction of TiO_2 under the influence of Ar^+ sputtering is a well-known phenomenon that is also observed here even a very low sputter energy of Ar^+ ions was used.^[25] Moreover, the reduced species of Ti^{3+} to Ti^{0+} in the TiO_2 film change the electronic properties and shift the Fermi level toward lower binding energy.

The Ti2p spectra from TCS-PES at both the interface of perovskite/ TiO_2 and TiO_2 layer have a single, strong $\text{Ti}2p_{3/2}$ peak at 458.9 eV corresponding to TiO_2 .^[43] The Ti2p intensity increases from the perovskite/ TiO_2 interface toward the TiO_2 layer showing the ability of TCS-PES to reach the front contact. Moreover, the Ti2p binding energy does not change from the interface to TiO_2 layer showing that there is no band bending at the perovskite/ TiO_2 interface, in agreement with the literature.^[20,27,29] The O1s spectra as measured by SDP-PES show a single peak at around 530.4 eV at the perovskite/ TiO_2 interface whereas two peaks are observed at around 530.4 and 532.5 eV for the TiO_2 layer corresponding to the metal oxide and metal hydroxide, respectively.^[62] In the O1s spectra taken with TCS-PES, two peaks located at 530.0 and 532.7 eV are visible and are attributed to the Ti—O bond in TiO_2 and to the —OH/—CO bonds.^[42,51] Here again, the adsorbed —OH or —CO groups are known to be present on the investigated sample surface using this method.^[29]

2.5. Electronic Properties

The PSC stack has combination of metal and semiconducting material layers. In the present case, the Ag is the metallic contact on the top and FTO at the bottom side where as the spiro-MeOTAD, perovskite absorber, and the TiO_2 are p-type, intrinsic, and n-type semiconducting layers, respectively. Difference in Fermi levels and chemical nature in all these layer cause changes in the chemical and electronic properties at the interface of each layer. Therefore, in the following section, we will discuss the electronic properties determined from the SDP- and TCS-PES measurements.

Figure 6 shows the contour plot of the $\text{Ag}3d_{5/2}$, C1s, $\text{Pb}4f_{7/2}$, Ti2p, and O1s core-level spectra with binding energy position marked in red of the main peaks investigated with a) SDP-PES and b) TCS-PES. In addition, yellow dashed lines mark the deviation in the binding energy position across the PSC stack. The Au/spiro interface makes an interface between the metal and p-type semiconductor. Depending on a type of contact (ohmic or Mott–Schottky) there can be a band bending at this interface. To explore the electronic properties of the Ag/spiro interface, we study the change in $\text{Ag}3d$ and C1s binding energy shift from the surface toward the bulk of the solar cell.

In SDP, the binding energy of the $\text{Ag}3d_{5/2}$ peak does not change with the sputtering time showing that it has no effect on the Ag film. Therefore, the $\text{Ag}3d_{5/2}$ binding energy can be used for the evaluation of the band bending at the Ag/spiro-MeOTAD interface. The binding energy of $\text{Ag}3d_{5/2}$ from the surface toward the bulk does not change. However, the sputtering changes the chemistry of the carbon (C1s) from spiro-MeOTAD (see Figure 4).

In the following, the C1s and $\text{Pb}4f$ core levels are used to understand if the band alignment at the spiro-MeOTAD/perovskite interface can be analyzed in the case of SDP measurements.

In the SDP-PES contour plot in Figure 6a, it can be seen that the C1s binding energy does not change till 40 min of sputtering; also the C1s core-level spectra, from the very first step of sputtering, loses the spectral features related to spiro-MeOTAD and the perovskite (see Figure 4a). In a case of SDP-PES, it is not possible to distinguish between the carbon spectra from spiro-MeOTAD and perovskite. Moreover, with prolonged sputtering, the metallic Pb states start to appear from the degradation of the perovskite at the spiro-MeOTAD/perovskite interface rendering the determination of the electronic properties of this interface ambiguous. Moving deeper from the spiro-MeOTAD/perovskite interface, the C1s peak first shifts to a higher binding energy and after 60 min of sputtering to a lower binding energy. A similar shift in binding energy is found in $\text{Pb}4f$, I3d, and Cs3d (Figure 2a and 6a) for SDP-PES. The shift here can be related to the chemistry of the intermixed spiro and perovskite layers. However, the spectral shape and feature show that the organic spiro and perovskite are destroyed by the Ar^+ during sputtering. Therefore, toward the TiO_2 layer the C1s shift to a higher binding energy may originate from the degradation of the perovskite, including the formation of lead halides.^[41] The shift toward lower binding energy after etching for 60 min is caused by the substrate effect. At this sputtering point the perovskite film gets thinner and the TiO_2 underneath gets reduced. The reduction of TiO_2 forms TiO_x which in turn changes the Fermi level of the layer and hence the position of the Ti2p position too. It shifts to lower binding energy (see Figure 5a). The spiro-MeOTAD/perovskite and perovskite/ TiO_2 interface cannot be determined from the SDP-PES method because, as we already described earlier, sputtering changes the chemistry and electronic properties of the organic and oxidic films.

In the TCS-PES results, it can be seen, that at point 4 in Figure 6b, where the spiro-MeOTAD is supposed to start, the C1s binding energy changes from 283.8 eV to higher binding energy (284.5 eV) toward the perovskite film. This means that the spiro-MeOTAD has a downward band bending of 0.7 eV toward perovskite (binding energy of C1s in spiro-MeOTAD bulk is 284.5 eV, and at the spiro-MeOTAD/perovskite interface is 283.8 eV). However, the presence of carbon contaminations may raise ambiguity in determining the band bending at spiro-MeOTAD/perovskite interfaces. The C1s has a binding energy around 285.0 eV that comes from carbon contamination. Considering possibility of similar amount of carbon contaminations on the tapered cross-section, the C1s peak at 285.0 eV should be visible throughout the complete tapered cross-section starting from Ag to TiO_2 layer. Surprisingly, the C1s on Ag and at spiro-MeOTAD layer has no strong intensity at 285.0 eV (see Figure 4) which shows that the external carbon contamination is minimal and that the C1s signal from respective layers is dominating. Therefore, we believe that the C1s spectra can be used as a signature for a band bending alignment across investigated device (starting from Ag/spiro-MeOTAD interface to perovskite/ TiO_2 interface). This shows that there is a band bending at spiro-MeOTAD/perovskite interface.

Also when moving from perovskite toward spiro layer the $\text{Pb}4f_{7/2}$ peak shift toward lower binding energy by 0.7 eV confirming the downward band bending. Therefore, both the C1s and $\text{Pb}4f$ show a downward band bending of 0.7 eV at the spiro-MeOTAD/perovskite interface. In the perovskite layer, the positions of both the C1s and $\text{Pb}4f_{7/2}$ peaks (138.5 eV) remain

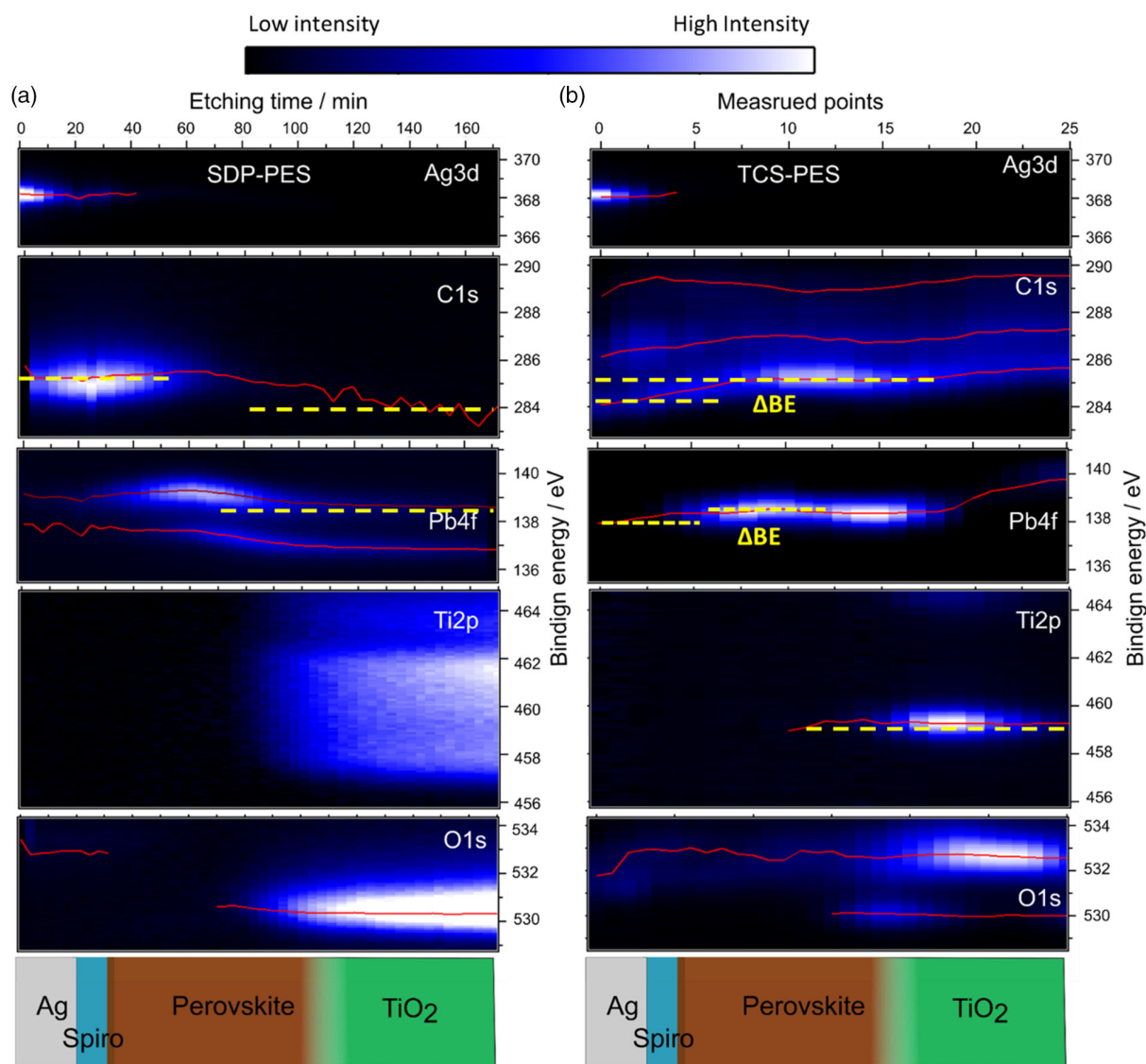


Figure 6. Contour plot of the Ag_{3d_{5/2}}, C_{1s}, Pb_{4f_{7/2}}, Ti_{2p}, and O_{1s} core-level spectra investigated using a) SDP-PES and b) TCS-PES methods. Red lines present on each contour plot indicate the binding energy position of the peaks. The yellow dashed lines mark the changes in the binding energy position across the PSC stack.

constant until the perovskite/TiO₂ interface is reached (point 15). A similar band bending has been reported by both TCS-PES and the classical sequential deposition interface experiments.^[20,27,29] At the front contact a sharp Ti_{2p_{3/2}} peak can be seen at 459.3 eV, and it does not change from the perovskite toward the TiO₂ layer (Figure 6b) confirming that there is no band bending at the perovskite/TiO₂ interface. Therefore, the TCS-PES shows that there is a downward band bending at the spiro-MeOTAD/perovskite interface and that the perovskite/TiO₂ interface is flat.

3. Conclusions

In summary, we have investigated the same PSC stack using two different top-down PES approaches. Namely, the SDP-PES and

TCS-PES were used to study the chemistry and electronic properties of the films and interfaces. Each of them has its advantages, but also disadvantages. The SDP-PES has an advantage over TCS-PES in terms of accuracy in layer-by-layer analysis. However, our research has shown that when using sputtering, even as gentle as 500 eV, to test the organic and oxidic materials that make up the PSC, we introduce artifacts. Namely, sputtering destroys the spiro-MeOTAD and perovskite layers, and changes the oxidation state of TiO₂. When using TCS-PES, we are limited by the dimension of the X-ray beam and spatial resolution. Also the TCS-PES probes the unaltered interior of a single layer giving better-quality results. No destructive ions are used for TCS-PES research; however, the method of preparation causes cross-contamination, and carbon, nitrogen, and oxygen appear in the PES spectra across the whole PSC stack. As in the PES

spectra, each chemical compound has its own binding energy, it is relatively easy to separate peaks that belong to the components of the PSC stack from those related to the contamination of the tested surface. The interfaces between the Ag/spiro-MeOTAD, spiro-MeOTAD/perovskite, and perovskite/TiO₂ layers can be identified with both methods.

Yet, the chemical and electronic properties of the interfaces can be investigated properly only using TCS-PES. The TCS-PES method shows that the band bending occurs only at the spiro-MeOTAD/perovskite interface, which exhibits a downward bending of about 0.7 eV toward the perovskite. Not shown in this study, but in our previous one,^[29] the TCS-PES is also able to investigate the chemical and electronic properties of the PCSs in operando.

Both methods have consistently revealed that the iodine migrates across the spiro-MeOTAD and accumulates in the Ag electrode. Also, it is found that the Br concentration is higher in the perovskite at the interface with mesoporous TiO₂ layer than with spiro-MeOTAD layer. Nevertheless, sputtering causes the creation of new chemical components in the investigated films. Also, the stoichiometry of the chemical elements in the individual layers is far away from the expected values in the SDP-PES results caused by the sputtered induced degradation. The atomic concentration of the chemical elements in the individual films agrees well with the expected values when the TCS-PES is used.

The TCS-PES can identify chemistry of the layers and interfaces and their electronic properties while the SDP-PES can identify the layer transition easily. For both chemical and electronic properties study of PSCs stack a combination of TCS-PES and SDP-PES will be more beneficial than the single method alone.

4. Experimental Section

Device Preparation: FTO substrates were first cleaned with 2% Hellmanex solution in water using a tooth brush and then sonicated in the same Hellmanex solution for 30 min. Then after substrates are rinsed with de-ionized water and were further sonicated in ethanol and isopropanol for 10 and 15 min, respectively. At the end of the cleaning process, each substrate was shortly rinsed in acetone and dried using a nitrogen gun. The substrates were further treated with UV-ozone for 15 min.

A 30 nm compact TiO₂ layer was deposited via spray pyrolysis using a precursor composed of 0.4 mL of acetylacetone and 0.6 mL of titanium diisopropoxide bis(acetylacetonate) stock solution (75 wt% in isopropanol) diluted in 9 mL of ethanol (Total 10 mL precursor solution for 30 substrates). The precursor solution was sprayed once the substrates reached a temperature of 450 °C and after spraying, the substrates were kept at this temperature for 45 min. Next to that, around 150–200 nm-thick mesoporous TiO₂ layer was spin coated at a speed of 4000 rpm for 20 s with a ramp of 2000 rpm s⁻¹, using a suspension of 30 nm TiO₂ particles paste in ethanol. After deposition, the substrates were dried at 120 °C followed by sintering at 450 °C for 30 min. The mesoporous TiO₂ layer was then doped with Li by spin coating 0.1 M solution of Li-TFSI in acetonitrile at 3000 rpm for 10 s and once again, the substrates were sintered at 450 °C for 30 min. The substrates were then quickly transferred to the glovebox once they were cooled down to 150 °C.

The perovskite precursor solution was prepared by mixing FAI (1 M), PbI₂ (1.1 M), MABr (0.2 M), and PbBr₂ (0.2 M) in anhydrous Dimethylformamide (DMF):Dimethyl sulfoxide (DMSO) 4:1 v.v. CsI solution of concentration 1.5 M was added in DMSO to this mixed perovskite precursor solution to obtain the desired triple cation composition. The composition used for these experiments was Cs_{0.05}(FA_{0.83}MA_{0.17})_{0.95}Pb(I_{0.83}Br_{0.17})₃. Sixty microliters of this perovskite solution was deposited on each substrate using a single-step program at 3000 rpm for 30 s. Hundred microliters of anisol was poured on the spinning substrate during the last 10 s. The substrates were then annealed at 100 °C for 45 min in a nitrogen-filled glovebox.

After the annealing step, the substrates were cooled down for few minutes and a spiro-OMeTAD solution (70 mM in anisol) was spin coated at 4000 rpm for 20 s. Spiro-MeOTAD was doped with bis(trifluoromethylsulfonyl)imide lithium salt (Li-TFSI) and 4-*tert*-butylpyridine (TBP). The molar ratios of additives for spiro-OMeTAD were 0.5 and 3.3 for Li-TFSI and TBP, respectively. After this, the substrates were kept over the night in a dry air atmosphere. Next day, 100 nm-thick silver electrodes were thermally evaporated under high vacuum to complete the device.

PES Characterization: The top-down PES investigation was done using the conventional SDP-PES and newly developed TCS-PES. For PES measurements, Thermo Fisher Scientific K-alpha system was used. The samples were excited with Al K-alpha X-ray (1486.6 eV) source. The data collection and the analysis were done using Avantage software from Thermo Fisher Scientific. For determination of binding energy of peak, the core level from SDP-PES and TCS-PES were fitted using Avantage and casaXPS software. During measurements, the Ag metal contact was grounded to the spectrometer leaving the TiO₂ of the solar cell stack floating. As the Ag is ground to the spectrometer the Ag3d can also be used as a reference for spectra analysis. For determination of atomic percentage, we used the Al Scofield factor which is of normal practice in XPS quantifications.

In **Figure 7a**, a sample after SDP-PES is shown. The SDP-PES was etched using low-energy (500 eV kinetic energy) Ar⁺-ion sputtering

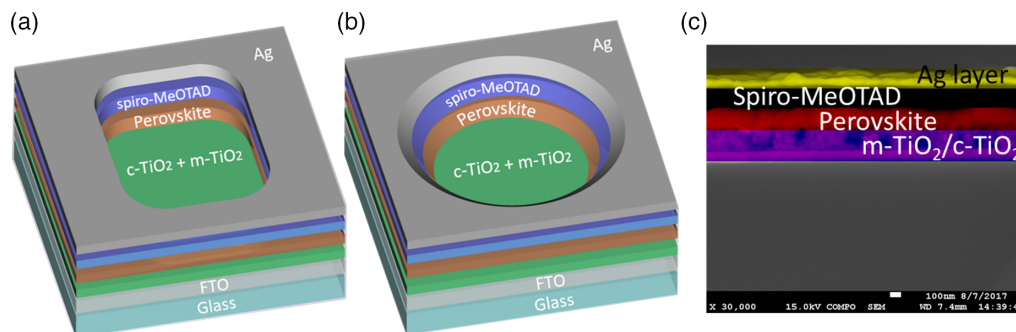


Figure 7. PSC stack view after PES investigation. a) The conventional Ar⁺ ion SDP-PES and b) the TCS-PES method. A cross-sectional SEM image of PSC is shown in (c).

system. In each step, 200 s of etching was done, and then the spectra were collected. In the case of SDP-PES the X-ray illumination spot was $400 \times 400 \mu\text{m}^2$.

A schematic diagram of TCS prepared on PSC is shown in Figure 7b. The TCS-PES was measured on a tapered cross-section prepared by a slight modification of the reported earlier method of preparation.^[27,29] We used a drilling machine to drill through the top of the sample using a conical cotton-polishing head on the drilling head. The diameter of the conical polishing head is 2.0 mm and a low rotation speed is used for drilling to avoid heating. A photographic presentation is shown Figure S3, Supporting Information. The soft drilling was done perpendicular to the surface of PSC, as shown in Figure S3, Supporting Information. The soft drilling process etched the PSC stack from Ag to TiO_2 layer mechanically. Then the sample was purged with argon gas to remove the dust on it. After the TCS preparation, the sample was taken to the spectrometer and PES measurement was carried out. Here, the X-ray illumination area was $50 \times 50 \mu\text{m}^2$ to make the higher spatial resolution. The width of the TCS measured was ≈ 3.0 mm. A measured step of $100 \mu\text{m}$ is used to avoid any overlapping measurement point along the line. Photographic image of both the TCS- and SDP-prepared trenches and the AFM at Ag/perovskite interface, on perovskite and TiO_2 are shown in Figure S4, Supporting Information.

Acknowledgements

We are thankful to Karlsruhe Nano Micro Facility (KNMF) for XPS. Open access funding enabled and organized by Projekt DEAL.

Conflict of Interest

The authors declare no conflict of interest.

Data Availability Statement

Research data are not shared.

Keywords

chemical distributions, depth profiles, interfaces, perovskite solar cells, X-ray photoelectron spectroscopy

Received: April 22, 2021

Revised: July 22, 2021

Published online: August 19, 2021

- [1] J. Chen, N. G. Park, *ACS Energy Lett.* **2020**, *5*, 2742.
 [2] S. Shao, M. A. Loi, *Adv. Mater. Interfaces* **2020**, *7*, 1901469.
 [3] Z. Qiu, N. Li, Z. Huang, Q. Chen, H. Zhou, *Small Methods* **2020**, *4*, 1.
 [4] M. I. Asghar, J. Zhang, H. Wang, P. D. Lund, *Renewable Sustainable Energy Rev.* **2017**, *77*, 131.
 [5] P. Schulz, E. Edri, S. Kirmayer, G. Hodes, D. Cahen, A. Kahn, *Energy Environ. Sci.* **2014**, *7*, 1377.
 [6] Q. K. Wang, R. Bin Wang, P. F. Shen, C. Li, Y. Q. Li, L. J. Liu, S. Duhm, J. X. Tang, *Adv. Mater. Interfaces* **2015**, *2*, 1.
 [7] G. F. Trindade, M. L. Abel, C. Lowe, R. Tshulu, J. F. Watts, *Anal. Chem.* **2018**, *90*, 3936.
 [8] S. P. Harvey, Z. Li, J. A. Christians, K. Zhu, J. M. Luther, J. J. Berry, *ACS Appl. Mater. Interfaces* **2018**, *10*, 28541.
 [9] V. W. Bergmann, S. A. L. Weber, F. Javier Ramos, M. K. Nazeeruddin, M. Grätzel, D. Li, A. L. Domanski, I. Lieberwirth, S. Ahmad, R. Berger, *Nat. Commun.* **2014**, *5*.
 [10] S. P. Harvey, J. Messinger, K. Zhu, J. M. Luther, J. J. Berry, *Adv. Energy Mater.* **2020**, *10*, 1903674, 1903674.
 [11] M. Kot, K. Henkel, K. Müller, L. Kegelman, S. Albrecht, N. Tsud, P. Kús, I. Matolinová, D. Schmeißer, *Energy Technol.* **2019**, *7*, 1900975.
 [12] F. Matteocci, Y. Busby, J. J. Pireaux, G. Divitini, S. Cacovich, C. Ducati, A. Di Carlo, *ACS Appl. Mater. Interfaces* **2015**, *7*, 26176.
 [13] S. Cacovich, G. Divitini, C. Ireland, F. Matteocci, A. Di Carlo, C. Ducati, *ChemSusChem* **2016**, *9*, 2673.
 [14] F. Matteocci, Y. Busby, J. J. Pireaux, G. Divitini, S. Cacovich, C. Ducati, A. Di Carlo, *ACS Appl. Mater. Interfaces* **2015**, *7*, 26176.
 [15] I. M. Hermes, Y. Hou, V. W. Bergmann, C. J. Brabec, S. A. L. Weber, *J. Phys. Chem. Lett.* **2018**, *9*, 6249.
 [16] M. Cai, N. Ishida, X. Li, X. Yang, T. Noda, Y. Wu, F. Xie, H. Naito, D. Fujita, L. Han, *Joule* **2018**, *2*, 296.
 [17] B. Wook Park, N. Kedem, M. Kulbak, D. Y. Lee, W. S. Yang, N. J. Jeon, J. Seo, G. Kim, K. J. Kim, T. J. Shin, G. Hodes, D. Cahen, S. Il Seok, *Nat. Commun.* **2018**, *9*, 1.
 [18] S. Béchu, M. Ralaarisoa, A. Etcheberry, P. Schulz, *Adv. Energy Mater.* **2020**, *10*, 1904007.
 [19] C. Das, M. Wussler, T. Hellmann, T. Mayer, W. Jaegermann, *Phys. Chem. Chem. Phys.* **2018**, *20*, 17180.
 [20] T. Hellmann, C. Das, T. Abzieher, J. A. Schwenzler, M. Wussler, R. Dachauer, U. W. Paetzold, W. Jaegermann, T. Mayer, *Adv. Energy Mater.* **2020**, *10*, 202002129.
 [21] B. Philippe, M. Saliba, J. P. Correa-Baena, U. B. Cappel, S. H. Turren-Cruz, M. Grätzel, A. Hagfeldt, H. Rensmo, *Chem. Mater.* **2017**, *29*, 3589.
 [22] R. Lindblad, N. K. Jena, B. Philippe, J. Oscarsson, D. Bi, A. Lindblad, S. Mandal, B. Pal, D. D. Sarma, O. Karis, H. Siegbahn, E. M. J. Johansson, M. Odelius, H. Rensmo, *J. Phys. Chem. C* **2015**, *119*, 1818.
 [23] C. Noël, S. Pescetelli, A. Agresti, A. Franquet, V. Spampinato, A. Felten, A. di Carlo, L. Houssiau, Y. Busby, *Materials* **2019**, *12*, 726.
 [24] Y. Busby, C. Noël, S. Pescetelli, A. Agresti, A. Di Carlo, J. Pireaux, L. Houssiau, *Phys. Chem. Semicond. Mater. Interfaces XVII* **2018**, *1072408*, 7.
 [25] K. Eom, U. Kwon, S. S. Kalanur, H. J. Park, H. Seo, *J. Mater. Chem. A* **2017**, *5*, 2563.
 [26] W. C. Lin, A. Kovalsky, Y. C. Wang, L. L. Wang, S. Goldberg, W. L. Kao, C. Y. Wu, H. Y. Chang, J. J. Shyue, C. Burda, *Phys. Chem. Chem. Phys.* **2017**, *19*, 21407.
 [27] C. Das, M. Wussler, T. Hellmann, T. Mayer, I. Zimmermann, C. Maheu, M. K. Nazeeruddin, W. Jaegermann, *ACS Appl. Mater. Interfaces* **2020**, *12*, 40949.
 [28] S. P. Harvey, F. Zhang, A. Palmstrom, J. M. Luther, K. Zhu, J. J. Berry, *ACS Appl. Mater. Interfaces* **2019**, *11*, 30911.
 [29] M. Wussler, T. Mayer, C. Das, E. Mankel, T. Hellmann, C. Prabowo, I. Zimmermann, M. K. Nazeeruddin, W. Jaegermann, *Adv. Funct. Mater.* **2020**, *30*, 201910679.
 [30] M. Kot, K. Wojciechowski, H. Snaith, D. Schmeißer, *Chem.—Eur. J.* **2018**, *24*, 3539.
 [31] M. Kot, L. Kegelman, H. Köbler, M. Vorokhta, C. Escudero, P. Kús, B. Šmíd, M. Tallarida, S. Albrecht, A. Abate, I. Matolinová, D. Schmeißer, J. I. Flege, *ChemSusChem* **2020**, *13*, 5722.
 [32] N. K. Kim, Y. H. Min, S. Noh, E. Cho, G. Jeong, M. Joo, S. W. Ahn, J. S. Lee, S. Kim, K. Ihm, H. Ahn, Y. Kang, H. S. Lee, D. Kim, *Sci. Rep.* **2017**, *7*, 1.
 [33] S. Svanström, A. García Fernández, T. Sloboda, T. J. Jacobsson, H. Rensmo, U. B. Cappel, *Phys. Chem. Chem. Phys.* **2021**, *23*, 12479.
 [34] C. Das, M. Wussler, T. Hellmann, T. Mayer, W. Jaegermann, *Phys. Chem. Chem. Phys.* **2018**, *20*, 17180.

- [35] A. I. Boronin, S. V. Koscheev, G. M. Zhidomirov, *J. Electron Spectrosc. Rel. Phenom.* **1998**, *96*, 43.
- [36] D. Briggs, *Handbook of Adhesion*, 2nd ed., John Wiley&Sons, Ltd, West Sussex **2005**, p. 621.
- [37] T. Hellmann, M. Wussler, C. Das, R. Dachauer, I. El-Helaly, C. Mortan, T. Mayer, W. Jaegermann, *J. Mater. Chem. C* **2019**, *7*, 5324.
- [38] X. Tang, M. Brandl, B. May, I. Levchuk, Y. Hou, M. Richter, H. Chen, S. Chen, S. Kahmann, A. Osvet, F. Maier, H.-P. Steinrück, R. Hock, G. J. Matt, C. J. Brabec, *J. Mater. Chem. A* **2016**, *4*, 15896.
- [39] Y. Li, X. Xu, C. Wang, B. Ecker, J. Yang, J. Huang, Y. Gao, *J. Phys. Chem. C* **2017**, *121*, 3904.
- [40] M. Deepa, M. Salado, L. Calio, S. Kazim, S. M. Shivaprasad, S. Ahmad, *Phys. Chem. Chem. Phys.* **2017**, *19*, 4069.
- [41] I. S. Zhidkov, A. I. Poteryaev, A. I. Kukharensko, L. D. Finkelstein, S. O. Cholakh, A. F. Akbulatov, P. A. Troshin, C. C. Chueh, E. Z. Kurmaev, *J. Phys. Condens. Matter* **2020**, *32*, 095501.
- [42] B. Bharti, S. Kumar, H. N. Lee, R. Kumar, *Sci. Rep.* **2016**, *6*, 1.
- [43] C. Das, M. Richter, M. Tallarida, D. Schmeisser, *J. Phys. D: Appl. Phys.* **2016**, *49*, 275304.
- [44] C. Das, M. Tallarida, D. Schmeißer, *Environ. Earth Sci.* **2013**, *70*, 3785.
- [45] C. Besleaga, L. E. Abramiuc, V. Stancu, A. G. Tomulescu, M. Sima, L. Trinca, N. Plugaru, L. Pintilie, G. A. Nemnes, M. Iliescu, H. G. Svavarsson, A. Manolescu, I. Pintilie, *J. Phys. Chem. Lett.* **2016**, *7*, 5168.
- [46] M. C. Brennan, S. Draguta, P. V. Kamat, M. Kuno, *ACS Energy Lett.* **2018**, *3*, 204.
- [47] C. Li, S. Tscheuschner, F. Paulus, P. E. Hopkinson, J. Kießling, A. Köhler, Y. Vaynzof, S. Huettner, *Adv. Mater.* **2016**, *28*, 2446.
- [48] T. Hellmann, M. Wussler, C. Das, R. Dachauer, I. El-helaly, C. Mortan, T. Mayer, *Mater. Chem. C* **2019**, *7*, 5324.
- [49] C. Das, M. Kot, T. Hellmann, C. Wittich, E. Mankel, I. Zimmermann, D. Schmeisser, M. Khaja Nazeeruddin, W. Jaegermann, *Cell Rep. Phys. Sci.* **2020**, *1*, 100112.
- [50] C. Das, K. Henkel, M. Tallarida, D. Schmeißer, H. Gargouri, I. Kärkkänen, J. Schneidewind, B. Gruska, M. Arens, *J. Vacuum Sci. Technol. A: Vacuum Surf. Films* **2015**, *33*, 01A144.
- [51] K. Henkel, C. Das, M. Kot, D. Schmeißer, F. Naumann, I. Kärkkänen, H. Gargouri, *J. Vacuum Sci. Technol. A: Vacuum Surf. Films* **2016**, *35*, 01B135.
- [52] P. Supphasrirongjaroen, W. Kongsuebchart, J. Panpranot, O. Mekasuwandumrong, C. Satayaprasert, P. Praserthdam, *Ind. Eng. Chem. Res.* **2008**, *47*, 693.
- [53] C. Das, M. Wussler, T. Hellmann, T. Mayer, W. Jaegermann, *Phys. Chem. Chem. Phys.* **2018**, *20*, 17180.
- [54] S. Malmgren, K. Ciosek, M. Hahlin, T. Gustafsson, M. Gorgoi, H. Rensmo, K. Edström, *Electrochim. Acta* **2013**, *97*, 23.
- [55] R. Hock, T. Mayer, W. Jaegermann, *J. Phys. Chem. C* **2014**, *116*, 1814.
- [56] B. Philippe, M. Saliba, J. P. Correa-Baena, U. B. Cappel, S. H. Turren-Cruz, M. Grätzel, A. Hagfeldt, H. Rensmo, *Chem. Mater.* **2017**, *29*, 3589.
- [57] J. D. P. Counsell, A. J. Roberts, W. Boxford, C. Moffitt, K. Takahashi, *J. Surf. Anal.* **2014**, *20*, 211.
- [58] S. Boyadzhiev, V. Georgieva, M. Rassovska, *J. Phys.: Conf. Ser.* **2010**, *253*, 012040.
- [59] M. Sowinska, T. Bertaud, D. Walczyk, S. Thiess, P. Calka, L. Alff, C. Walczyk, T. Schroeder, *J. Appl. Phys.* **2014**, *115*, 1.
- [60] M. Sowinska, T. Bertaud, D. Walczyk, S. Thiess, M. A. Schubert, M. Lukosius, W. Drube, C. Walczyk, T. Schroeder, *Appl. Phys. Lett.* **2012**, *100*, 233509.
- [61] Y. Sakai, S. Ninomiya, K. Hiraoka, *Surf. Interface Anal.* **2011**, *43*, 1605.
- [62] P. Supphasrirongjaroen, W. Kongsuebchart, J. Panpranot, O. Mekasuwandumrong, C. Satayaprasert, P. Praserthdam, *Ind. Eng. Chem. Res.* **2008**, *47*, 693.